Journal of
Marine Science and Engineering

MDPI

Article

Provenance of the Lower Jurassic Badaowan and Sangonghe Formations in Dongdaohaizi Depression, Junggar Basin, and Its Constraint on the Karamaili Ocean

Yangjun Gao [1], Guanlong Zhang [1], Songtao Li [1], Ruichao Guo [1], Zhiping Zeng [1], Shiwei Cheng [1], Zelei Xue [1], Ling Li [1], Huilian Zhou [1], Shengqian Liu [2] and Furong Li [1,3,*]

1 Exploration and Development Research Institute, Shengli Oilfield, Sinopec, Dongying 257000, China
2 Key Laboratory of Exploration Technologies for Oil and Gas Resources, Yangtze University, Ministry of Education, Wuhan 430100, China
3 State Key Laboratory of Nuclear Resources and Environment, East China University of Technology, Nanchang 330013, China
* Correspondence: furongli@ecut.edu.cn

Abstract: The Paleo-Asian Ocean controlled the tectonic evolution of Northeast Asia and formed the Karamaili Orogenic Belt in the eastern Junggar basin. However, the chronological constrain of the evolution of the paleo-Karamaili Ocean remains unclear. In this study, we focused on the sandstones of the Lower Jurassic Badaowan and Sangonghe Formations in the Dongdaohaizi Depression, Junggar basin near the Karamaili orogenic belt. After detailed observations and descriptions of the macroscopic features of the sandstone, we obtained information on petrology and geochronology. The Dickinson diagrams indicate that the provenance area had the characteristics of a transitional and recycling provenance, which is a collisional orogenic belt with a background of oceanic-continental subduction. The detrital zircon ages of the Lower Jurassic sediments in the Dongdaohaizi Depression can be divided into three peaks: ~300 Ma, ~420 Ma, and ~510 Ma for Badaowan Formation and ~310 Ma, ~410 Ma, and ~500 Ma for Sangonghe Formation. The youngest detrital zircon age is 241 ± 2 Ma, representing an Early Permian depositional age. Combined with previous studies, the sediments in the study area represent a provenance from the Karamaili Ocean. During the Early Jurassic, the consistent subduction of the residual East Junggar Ocean induced continuous uplift in the Karamaili region, resulting in an increasing exposure of deep-seated rocks to provide sedimentary material. According to the tectonic background of the Junggar region, the results indicate that the Karamaili Ocean, as part of the Paleo-Asian Ocean, experienced three evolutionary stages: Cambrian-Early Silurian (460–540 Ma), Late Silurian-Early Carboniferous (360–440 Ma), and Late Carboniferous–Triassic (240–340 Ma).

Keywords: provenance; detrital zircon; Junggar basin; Karamaili Ocean; Early Jurassic

check for updates

Citation: Gao, Y.; Zhang, G.; Li, S.; Guo, R.; Zeng, Z.; Cheng, S.; Xue, Z.; Li, L.; Zhou, H.; Liu, S.; et al. Provenance of the Lower Jurassic Badaowan and Sangonghe Formations in Dongdaohaizi Depression, Junggar Basin, and Its Constraint on the Karamaili Ocean. *J. Mar. Sci. Eng.* **2023**, *11*, 1375. https://doi.org/10.3390/jmse11071375

Academic Editors: George Kontakiotis, Assimina Antonarakou and Dmitry A. Ruban

Received: 14 June 2023
Revised: 3 July 2023
Accepted: 3 July 2023
Published: 5 July 2023

1. Introduction

The evolution of the Paleo-Asian Ocean between the Siberian Plate and the Amur-North China and Tarim Plates controlled the growth and transformation of the northeastern Asian continent, forming the significant continental orogenic belt known as the Central Asian Orogenic Belt (Figure 1a) [1–5]. The Paleo-Asian Ocean underwent multiple stages of tectonic evolution, involving periods from the Precambrian to the Mesozoic, and has always been the focus of scholars' attention [6–10].

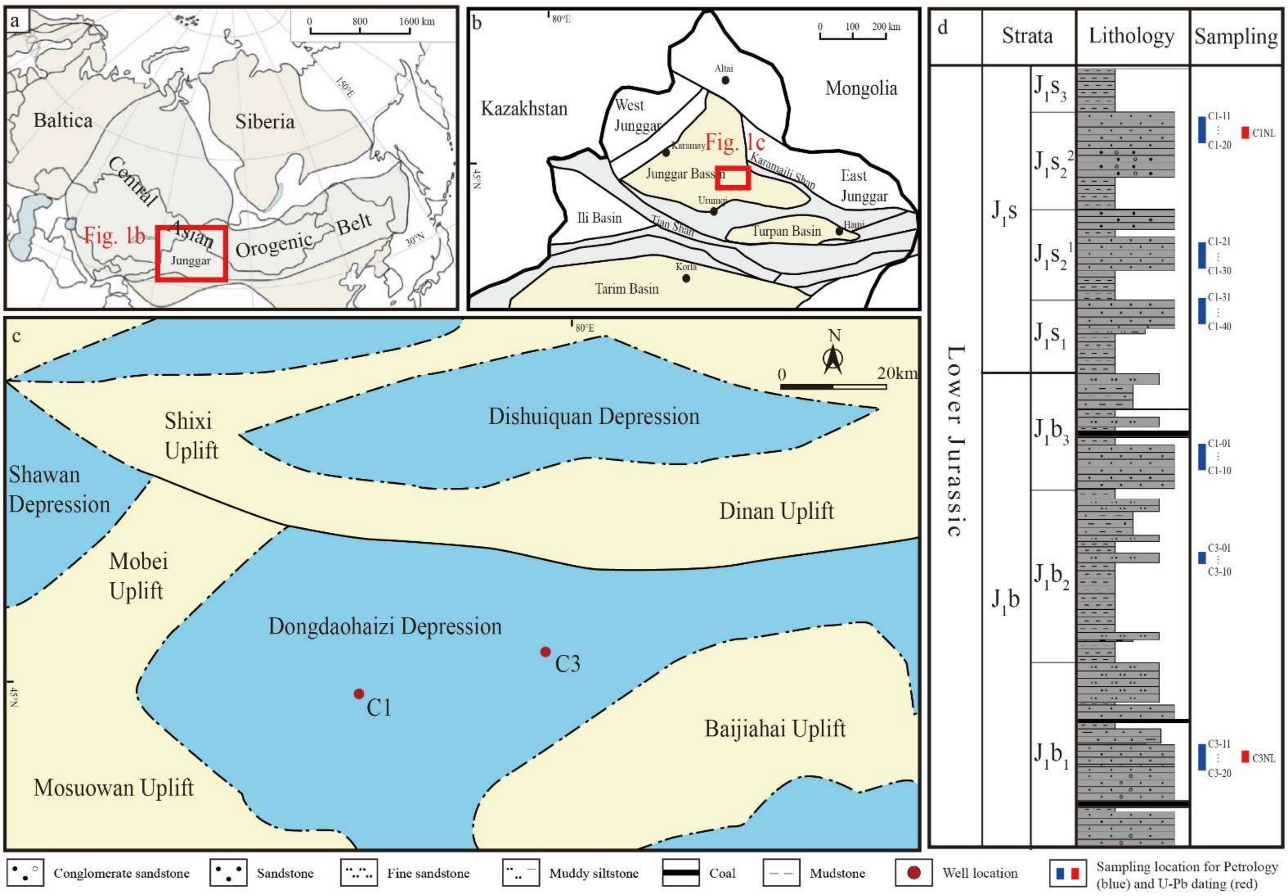

Figure 1. (**a**–**c**) Geological map of Eurosia Plate, Junggar Basin, and Dongdaohaizi area, respectively. (**d**) Chronostratigraphy and lithology section of Lower Jurassic in Dongdaohaizi Depression. Abbreviations: J_1b = Lower Jurassic Badaowan Formation, J_1s = Lower Jurassic Sangonghe Formation.

The Karamaili Ocean is located between the Kazakhstan-Junggar and Siberian plates and is an important branch of the Paleo-Asian Ocean. Its subduction represents the subduction, collision, and accretion of the Junggar-Tairm block onto the Siberian plate, forming the Karamaili tectonic belt in the eastern Junggar area (Figure 1b) [6,7,11–14]. Investigating the evolutionary history of the Karamaili Ocean provides valuable insights into the broader evolution of the Paleo-Asian Ocean.

Previous studies on the Karamaili Ocean are mainly based on the outcrops of the eastern Junggar orogenic belt. The outcrops are limited, dispersed, heavily fragmented, and subjected to significant metamorphism and deformation by the intense tectonic activity of the orogenic belt, resulting in highly disputed chronological constraints for the evolution of the Karamaili Ocean. For example, the duration and the timing of the final closure of the Karamaili Ocean have been a topic of debate in the geological community due to the varying ages reported by different methods and data sources, ranging from the Late Devonian to the Late Permian. Some studies have employed geochronological data to suggest a Late Carboniferous or Early Permian closure of the Karamaili Ocean, based on the ages of ophiolites, arc magmatism, and collisional granites along the suture zone [15–17]. In other studies, paleomagnetic data have been utilized in some studies to support a Late Devonian or Early Carboniferous closure of the Karamaili Ocean, citing the similarity of paleolatitudes between Siberia and Tarim [18–20]. Therefore, more reliable data reflecting the overall evolutionary development of the ocean basin are needed.

The subduction of the ocean basin transported a large amount of ocean basin volcanic and clastic material from the ocean-land boundary to the basin through the source-sink system [21]. By comparing the properties of sediments in the stable continental basin nearest to the margin where the ocean basin closed, we can obtain a complete understanding of the transformation history of the ocean.

The Junggar Basin was formed by the assemblage of volcanic island arcs and accretionary wedges and was a stable basin with a Paleozoic basement in the early Jurassic. The Dongdaohaizi Depression is located in the eastern part of the Junggar Basin, adjacent to the orogenic belt of eastern Junggar, and has incorporated a large amount of sediment from the ancient ocean during the basin-margin orogeny (Figure 1b,c). According to a recent study [22], a large number of shallow braided rivers developed in the basin during the Early to Middle Jurassic, with sediment from the basin margin being transported more than 200 km, effectively ensuring the breadth and volume of the sediment supply.

Currently, quantitative analysis has become the main direction of provenance analysis. Through U-Pb isotopic dating analysis of characteristic minerals such as zircons, geological activities of the source region for the clastic sediments present in the Dongdaohaizi depression can be examined [23]. Therefore, this study takes the deep-drilling cores of the Lower Jurassic Badaowan Formation and Sangonghe Formation sandstones in the Dongdaohaizi Depression as the research object. Based on the study of petrological characteristics in combination with the LA-ICP-MS detrital zircon U-Pb geochronological study, the age characteristics of the Badaowan and Sangonghe formations were determined, and the provenance characteristics and the evolution of the Karamaili Ocean were further revealed accordingly.

2. Geological Setting and Sampling

The Junggar Basin is located in the northern part of Xinjiang, China, at the intersection of the Kazakhstan Plate, Siberian Plate, and Tarim Plate, and is the eastward extension of the Kazakhstan Plate (Figure 1a,b) [24,25]. The basin is generally wider in the south and narrower in the north and has a triangular distribution, consisting of the primary tectonic units of the Ulungur Depression, Luliang Uplift, Central Depression, eastern Uplift, western Uplift, and Southern Margin Thrust Belt. The Dongdaohaizi Depression belongs to the secondary tectonic unit of the central depression of the Junggar Basin. The study area is located in the middle of the Dongdaohaizi Depression, with the Mosuowan Uplift to the west, the Baijiahai Uplift to the east, and the Fukang Depression to the south (Figure 1c). The Dongdaohaizi Depression was formed in the early stage of the Hercynian period and developed a large set of marine shales and marls with widespread distribution of calc-alkaline volcanic rocks. Strong earthquake and volcanic activity, accompanied by faulting, occurred in the Early Carboniferous to Early Permian, providing the basis for the internal structure of the central depression [26]. The structures in the study area mainly developed in the Devonian basement. The basement is then covered with a huge thickness of Mesozoic (>5000 m) and Cenozoic (>3000 m) rocks. the tectonic movements during the Late Hercynian and Yanshanian played a decisive role in the structural deformation of the study area [27]. Interlayer faults trending nearly northeast, dominated by normal faults with a short horizontal extension developed during the Jurassic.

The Jurassic strata in the Dongdaohaizi Depression include the Badaowan Formation, Sangonghe Formation, Xishanyao Formation, and Toutunhe Formation, while the Qigu Formation is not developed in this area. Among them, the Badaowan Formation, Sangonghe Formation, and Xishanyao Formation include coal-bearing strata. The Xishanyao Formation is mainly composed of fluvial deposits, with sandstone thickness accounting for 50% of the stratum thickness. The maximum thickness of a single layer is 14 m, and the general thickness ranges from 2 m to 8 m, with significant lateral thickness variations. The Toutunhe Formation is dominated by continental (lake-swamp) deposits and is composed of sandstone, red and gray sandy mudstone in ascending order.

The Lower Jurassic Badaowan Formation and Sangonghe Formation are the target intervals of this study in the Dongdaohaizi Sag area (Figure 1d). The Badaowan Formation is primarily composed of fluvial and deltaic deposits. Sandstone beds account for 45% of the formation thickness, with a maximum single-layer thickness of 30 m and a general thickness range of 4 m to 22 m. The Badaowan Formation exhibits distinct cyclicity, with a coarse-fine-coarse sequence from bottom to top. The lithological assemblage consists mainly of conglomerate, sandstone, mudstone, and coal seams. In the Early Jurassic, the Indosinian movement, caused by the collision of eastern Asia blocks, led to the formation of the Sikezhuang Sag, resulting in a regional angular unconformity between the Jurassic and Triassic strata. The sedimentary center during the deposition of the Lower Jurassic Badaowan Formation was located in the Changji Sag and the Penyijingxi Sag, with a maximum thickness of 1200 m. The lithology of the formation can be divided into two parts: the upper part is composed of interbedded mud and sand, and the middle and lower parts are composed of gray-green or gray-black mudstone interbedded with conglomerate or pebbly sandstone. The Badaowan Formation is the first major coal-bearing formation developed in the Junggar Basin and also constitutes the first major hydrocarbon source rock and reservoir in the basin. The first and third members of the Badaowan Formation are mainly sandstone, while the second member is mainly mudstone.

The Sangonghe Formation is primarily composed of gray sandstone, fine-grained sandstone, and mudstone containing siltstone, with tuff and quartz as the dominant sandstone, followed by feldspar, with small amounts of illite and smectite minerals. The sandstones exhibit moderate-to-well sorting and sub-angular to sub-rounded grains, and the mudstone-calcium mudstone facies shows a matrix-supported texture. The sandstone layers account for 37% of the formation thickness, with a maximum single-layer thickness of 14 m and a general thickness range of 2 m to 10 m. The sedimentary environment is primarily deltaic deposits, and it is similar to the sedimentary area of the Badaowan Formation. The sedimentary center was located in the central Junggar Basin, and the sedimentary thickness was also approximately 1200 m. The lithology of the formation can be divided into two parts: the middle and upper members are interbedded sand-mudstone, and the lower member is composed of medium-grained conglomerate and sandstone rocks, forming the main hydrocarbon source rock and reservoir Jurassic in the Junggar Basin.

In this study, 60 samples were collected from lower Jurassic Badaowan and Sangonghe Formations for petrological and whole-rock analysis (Figure 1d, blue bars; Table S1). Samples C1-1 to C1-10 were collected from Badaowan Formation upper member sandstones at well C1; samples C3-1 to C10 were collected from Badaowan Formation middle member fine sandstones at well C3; samples C3-11 to C3-20 were collected from Badaowan Formation lower member sandstones at well C3; samples C1-11 to C1-20 were collected from Sangonghe Formation middle member upper sub-member sandstones at well C1; samples C1-21 to C30 were collected from Sangonghe Formation middle member lower sub-member sandstones at well C1; samples C1-31 to C40 were collected from Sangonghe Formation lower member sandstones at well C1. In addition, samples C1NL and C3NL were collected from Sangonghe Formation middle member upper sub-member sandstones at well C1 and Badaowan Formation lower member sandstones at well C3 for detrital zircon U-Pb dating (Figure 1d, red bars; Table S2).

3. Petrology and Methods

3.1. Petrologic Characteristics

Samples from Badaowan and Sangonghe formations are mainly medium-fine sandstones (Figures 1d and 2a). The detrital components of the formations are mainly composed of quartz, feldspar, and lithic fragments. The sandstone structures are well-developed, with sub-angular to sub-rounded grains and moderate sorting. The types of cement are diverse, with mudstone being the dominant matrix, while calcite is the main cement mineral, with occasional occurrences of dolomite. The primary mode of cementation is compactional cementation.

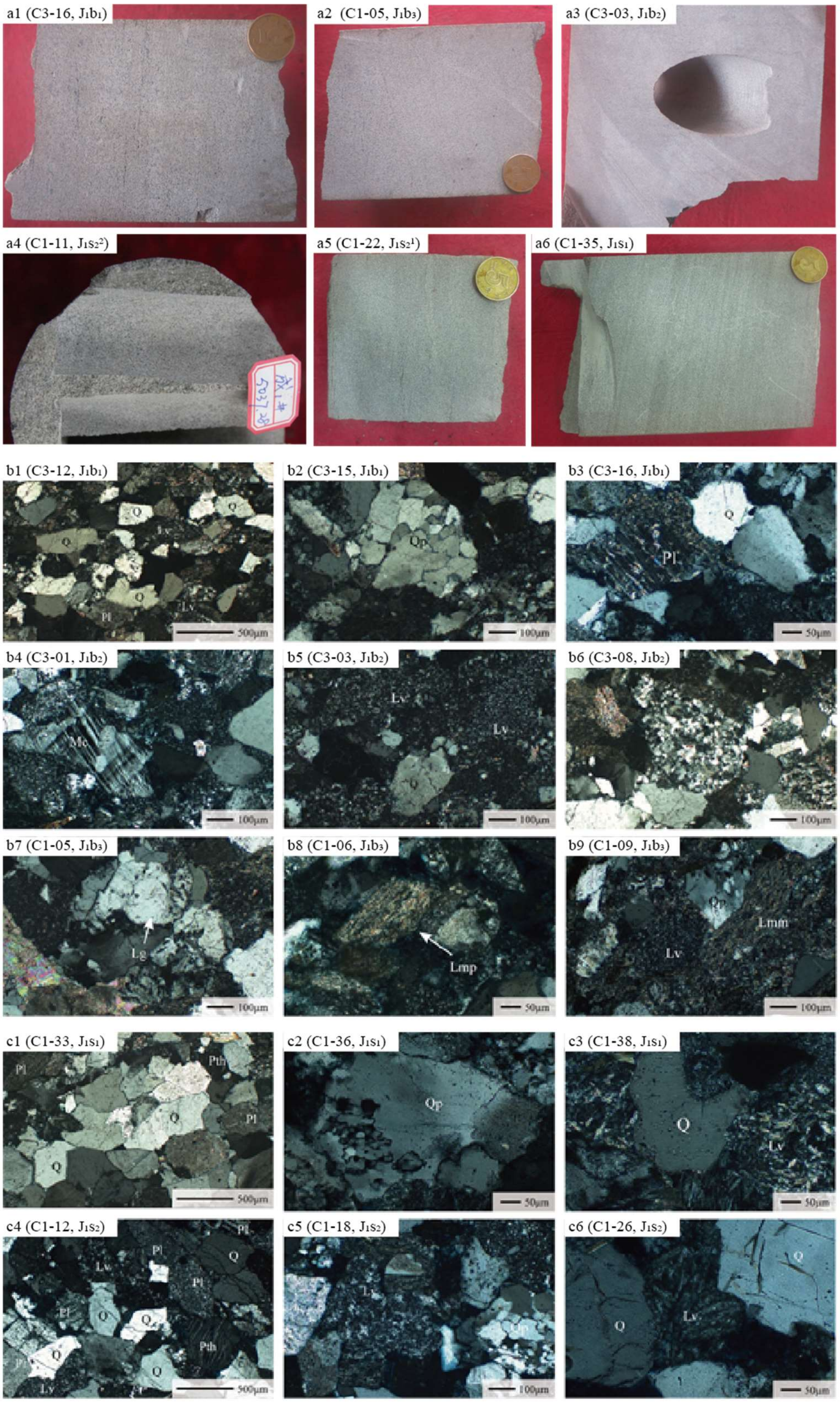

Figure 2. (**a**) Representative photograph of sandstone samples from Badaowan Formation (**a1**–**a3**) and Sangonghe Formation (**a4**–**a6**), respectively. Cross-polarized light photomicrograph of sandstone samples from Badaowan Formation (**b1**–**b9**) and Sangonghe Formation (**c1**–**c6**), respectively. Q = quartz, Qp = polycrystalline quartz; Pl = plagioclase, Mc = microcline, Lv = volcanic rock fragments, g = granite clasts, Lmp = quartz-mica schist clasts, Lmm = slate clasts, Pth = perthitic feldspar.

Based on mineralogical analyses of slices of the Badaowan and Sangonghe Formations, the components and their proportions are summarized in Table S1. The compositional features of the detrital rocks in the study area were analyzed in conjunction with observations of the samples and slices. The samples are mainly grey, feldspathic litharenite with a fine to medium grain size and blocky structure (Figure 2(a1–a3)). Quartz is one of the main detrital components in the sandstones of the study area, with a content range of 40% to 60%. It is well-rounded and mature, with angular to sub-angular shapes being common (Figure 2(b1)). Single crystal and polycrystalline quartz grains are also present (Figure 2(b2)), with some exhibiting undulose extinction. Feldspar content ranges from 12% to 20%, with sub-angular shapes being common. Plagioclase and potassium feldspar are the main types of feldspar present, with widespread alteration and a dirty appearance. Sericite and kaolinite are also abundant, with polysynthetic twins visible in some plagioclase grains (Figure 2(b3)) and grid twinning visible in some microcline grains (Figure 2(b4)). The lithic fragment content is typically 30% to 40%, with volcanic lithic fragments being the most common, especially tuffaceous lithic fragments. Sedimentary and metamorphic lithic fragments are less common, with occasional occurrences of mudstone, shale, quartzite, and phyllite lithic fragments (Figure 2(b5–b9)). Tuffaceous lithic fragments are composed of angular to sub-angular feldspar and quartz crystals with varying degrees of devitrification. Chert lithic fragments are mainly composed of microcrystalline or cryptocrystalline quartz. Phyllite lithic fragments are mainly composed of sericite, with a schistose texture and phyllitic structure.

The lithological and mineralogical characteristics of the Sangonghe Formation in the study area were summarized and analyzed based on the thin section data (Table S1). Microscopic observations reveal that the Sangonghe Formation is predominantly composed of plagioclase-rich lithic sandstone, lithic sandstone, and minor plagioclase-lithic sandstone. The lithic fragments are dominated by igneous and metamorphic rocks, and exhibit medium to fine grain size and blocky texture. Quartz, which accounts for 30% to 50% of the Sangonghe Formation, shows angular to sub-angular shapes with straight to concave-convex contacts, and some quartz grains exhibit secondary enlargement (Figure 2(c1)), undulose extinction, and embayment structures, indicating their derivation from igneous rocks (Figure 2(c2,c3)). Feldspar fragments, including plagioclase, striped feldspar, and potassium feldspar, exhibit dirty surfaces and widespread alteration, with intense sericitization and clay mineralization (Figure 2(c3)).

The lithic components of the Sangonghe Formation sandstones are predominantly composed of igneous and metamorphic rocks, indicating a low compositional maturity and a short transport distance, which suggests a control from the eastern Karamaili Mountain provenance. Some samples mainly consist of lithic sandstone, with igneous rock lithic fragments as the main component and low compositional maturity, indicating a short transport distance and control from the eastern Karamaili Mountain provenance. Microscopic observations also reveal abundant tuffaceous lithic fragments and a small amount of basaltic lithic fragments in the Sangonghe Formation (Figure 2(c5,c6)). Overall, the Sangonghe Formation samples have a lower lithic content and tuffaceous lithic content than the Badaowan Formation and exhibit higher porosity.

3.2. Methods

3.2.1. Zircon U-Pb Dating

Samples C1NL (~2 kg) and C3NL (~2.5 kg) were collected, and samples with relatively uniform color and lithology were selected. These samples were sent to Chengxin Geological Services Company in Langfang, Hebei for zircon separation to obtain sufficient zircons for testing and analysis. The zircons were made into targets at Beijing Zirconia Navigation Technology Co., Ltd., Beijing, China. The zircon samples were then subjected to transmitted and reflected light and Cathodoluminescence (CL) photography to observe their structure. The choice of CL images for the analysis is the Chromal CL 2 cathodoluminescence probe, which is configured on the JEOL JSM-6510A scanning electron microscope. The analysis conditions are as follows: acceleration voltage of 10 kV, beam current of SS65, and a working distance of 14 mm. These experiments were worked out at the Experimental Center of the School of Earth Sciences, Yangtze University.

The zircon U-Pb isotopic dating analysis was conducted at the Experimental Center of the School of Earth Sciences, Yangtze University. The NWR193HE laser ablation system (Elemental Scientific Lasers LLC, Bozeman, MT, USA) produced by ESI in the United States was used. The isotope ratios and element contents of the samples were calculated using the GLITTER program (ver4.0, Macquarie University), and the common Pb correction was performed using the method developed by Andersen [28].

Due to the presence of a large amount of radiogenic Pb in some zircons, the $^{207}Pb/^{206}Pb$ surface age was used for detrital zircons with U-Pb ages greater than 1000 Ma, while the $^{206}Pb/^{238}U$ surface age was used for zircons with U-Pb ages less than 1000 Ma [29,30]. The age-weighted average and age concordia diagram were calculated using the Isoplot program [31]. The standard deviation of single measurements of zircon U-Th-Pb isotope ratios and age data was 2σ, and the weighted average age was calculated using 2σ.

3.2.2. Whole-Rock Analysis

The composition of rock fragments is a direct expression of the combination of rock types and properties of source rocks. Microscopic analysis of the rock fragment composition in a study area can, to a certain extent, match the composition of the detrital material from the source rocks. The Dickinson triangle diagram is a widely used method for source rock discrimination studies, which can determine the properties of the source rocks and their tectonic background by analyzing the sandstone fragment composition, including the content of quartz, feldspar, and lithic fragments. In this study, we analyzed the component characteristics of the detrital rock samples from the study area by using the Dickinson triangle diagram based on the statistical analysis of the detrital zircon particles in the samples.

Fine-grained, medium-coarse-grained, and coarse-grained sandstone samples were selected from the specimens, and the weathered surface layer was removed first. The fresh rock portions were then made into thin rock sections. The square mesh intersection method was used to statistically count the detrital particles [32], and the statistical method of Gazzi-Dickinson was referenced [33,34]. The ternary provenance diagram in the Gazzi-Dickinson method aims to determine the provenance of the clastic material in analyzed sandstones. Provenance diagrams show percentage ratios of monomineral quartz, feldspar, and lithic fragments in each analyzed sample. Based on their composition, samples are plotted in different provenance areas. To ensure the accuracy of the results, samples with a matrix volume fraction greater than 25% were excluded from the statistical and plotting analyses, and the average particle size of the sandstone samples included in the statistics and plot analysis was limited to between medium-coarse-grained (including conglomerate) and arithmetic particle size 0.2–2 mm. The rock samples were used only for reference, and statistical errors due to the influence of detrital particle size on mineral composition properties were minimized as much as possible. A total of 300–400 statistical points were used for each thin section, and the caliper was used to control the spacing during the counting process. The grid spacing was twice the average particle size. In other words, a particle point was counted every time the caliper was moved along the same measurement line by a distance of twice the average particle size. After counting one line, the caliper was moved vertically by a distance of twice the average particle size, and the second line was counted, and so on. The counted detrital particle types included single-crystal quartz, polycrystalline quartz, plagioclase, potassium feldspar, sedimentary rock debris, metamorphic rock debris, volcanic rock debris, and secondary mineral particles such as mica, hornblende, and epidote. The specific types of detrital particles and their modal contents are shown in Table 1.

Table 1. Detrital particle compositions and calculation of detrital particles.

Detrital Particle Composition	Calculation of Detrital Particles
Q = Qm + Qp = total quartz Qm = monocrystalline quartz Qp = poly-crystalline quartz	QFL%Q = 100 × Q/(Q + F + L) QFL%F = 100 × F/Q + F + L) QFL%L = 100 × L/(Q + F + L) QmFLt%Qm = 100 × Qm/(Qm + F + Lt)
F = total feldspar	
Lt = L + Qp = total lithic content L = Ls + Lm + Lv = total unstable lithic fragments Ls = sedimentary lithic fragments Lm = metamorphic lithic fragments Lv = volcanic lithic fragments	

Note: Q = total monocrystalline (Qm) and polycrystalline (Qp) quartz grains; F = total potassium feldspar (K) and plagioclase (P) grains; L = aphanitic unstable lithic grains, including sedimentary (Ls), metamorphic (Lm) and volcanic (Lv) fragments.

4. Results

4.1. Badaowan Formation

The zircon morphology of the sandstone from the Badaowan Formation is mainly short columnar and irregular grains, with a grain size ranging mostly from 70 to 180 μm and an average size of 126 μm. Most of the zircons are angular, but some are well-rounded, suggesting that they may have been transported over a long distance. Cathodoluminescence (CL) images of the zircons from the Badaowan Formation reveal that most zircons have weak luminescence and typical oscillatory zoning features, indicating that they are mainly magmatic zircons (Figure 3a). The Th/U values of the zircons are generally greater than 0.4, with a range of 0.4–1.6. Zircons with a Th/U ratio greater than 0.4 accounts for approximately 90% of the zircons (Table S2), reflecting their magmatic origin. However, a few zircons exhibit strong cathodoluminescence intensity without zoning or with weak or patchy zoning (Figure 3a), indicating that they are metamorphic zircons. A small number of zircons also have Th/U values less than 0.1, reflecting their metamorphic origin, while others have Th/U values between 0.1 and 0.4 (Table S2).

The valid zircon U-Pb ages from Badaowan Formation are mainly at a range of 200–600 Ma, with a concordance of more than 94% (Figure 4a). Detrital zircon ages display three prominent peaks on the U-Pb age spectrum: 280–330 Ma, 400–440 Ma, and 490–520 Ma (Figure 4b), with a minimum age of 241 ± 2 Ma and a maximum age of 1992 ± 17 Ma (Figure 4a and Table S2). The detrital zircons are mainly derived from the Permian and Devonian, followed by the Cambrian, Carboniferous, and Silurian, with a few Triassic and Proterozoic zircons.

The sandstones from the Badaowan Formation are concentrated in a relatively narrow area. The QmFLt ternary diagram shows that the samples are mainly distributed in the transitional and back-arc source regions, with a few falling on the edges of the accretionary orogenic and transitional arcs, indicating that the source region contains a large number of volcanic rocks and intermediate to acidic intrusive rocks (Figure 5a). On the QtFL ternary diagram, the samples are mainly distributed in the recycled orogenic source region, with a larger proportion of oceanic material and a center of gravity that leans towards oceanic material, indicating that the source region is a collisional suture or fold-thrust belt (Figure 5b). The QmFLt auxiliary diagram indicates that the provenance area is basically a recycled orogenic belt, and the high chert-to-quartz ratio indicates that the provenance area belongs to the collision suture zone or fold-thrust zone (Figure 5c). The QpLvLs ternary diagram suggests that the sandstone samples are almost all from the collisional suture zone and fold-thrust belt source region, based on the high ratio of quartz to feldspar (Figure 5d).

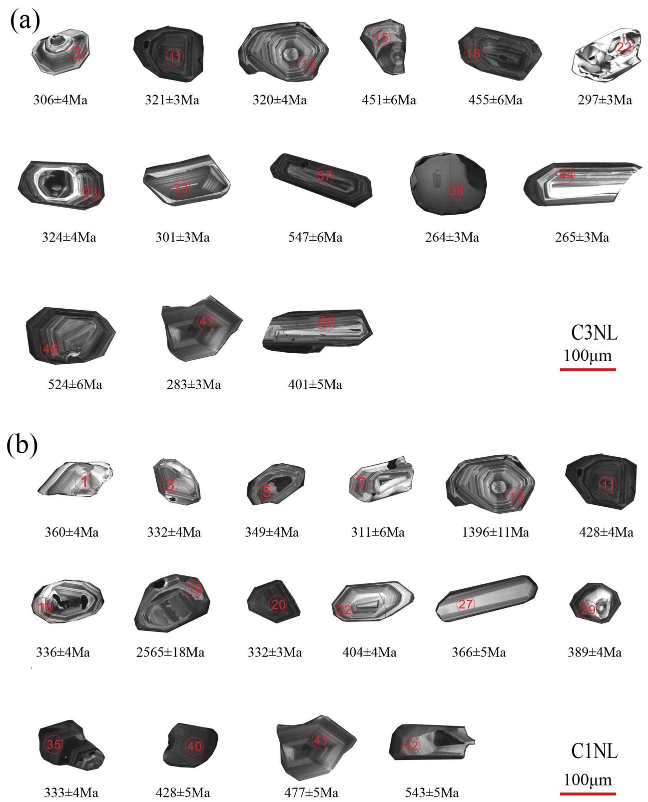

Figure 3. (**a**,**b**) Representative detrital zircons of Badaowan and Sangonghe Formation samples, respectively.

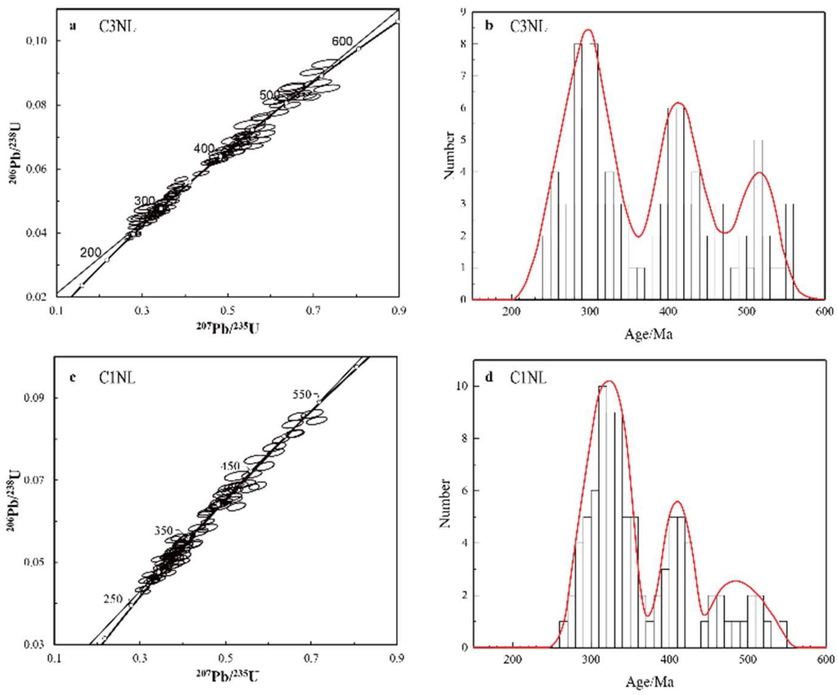

Figure 4. (**a**,**b**) Concordia diagram showing zircon LA-ICPMS U-Pb dating results and histogram of the detrital zircon ages for Badaowan Formation, respectively. (**c**,**d**) Concordia diagram showing zircon LA-ICPMS U-Pb dating results and histogram of the detrital zircon ages for Sangonghe Formation, respectively. Data are shown in Table S2.

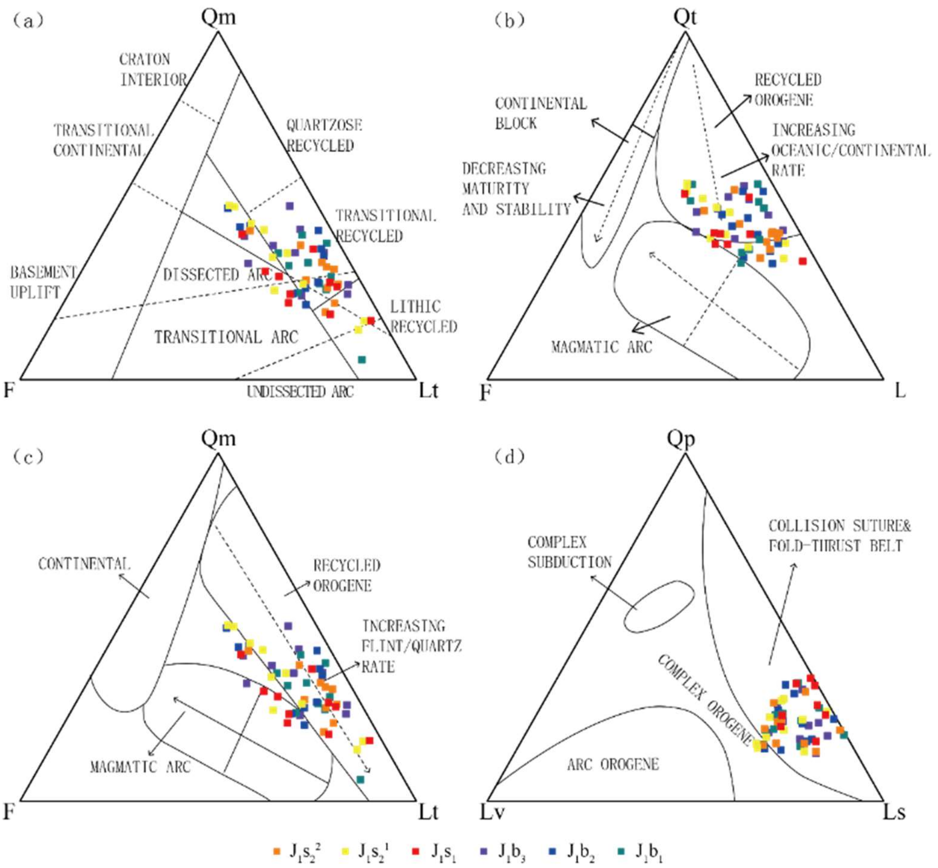

Figure 5. The (**a**) Qm-F-Lt, (**b**) Qt-F-L, (**c**) Qm-F-Lt and (**d**) Qp-Lv-Ls ternary plots of relative proportions of framework-grain compositions for sandstones from Badaowan and Sangonghe Formations in Dongdaohaizi Depression. The data and abbreviations are shown in Table S1.

4.2. Sangonghe Formation

The zircon morphology of the sandstones from the Sangonghe Formation is mainly short-columnar and irregular-granular, with some zircons showing good rounding and indicating long-distance transportation (Figure 3b). The average grain size is 120 μm, and the majority of zircons exhibit typical oscillatory zoning, suggesting magmatic origin with a Th/U ratio greater than 0.4. The Th/U ratio of zircons from the Sangonghe Formation ranges from 0.4 to 1.8, with about 90% of zircons having a ratio greater than 0.4 (Table S2). A small number of metamorphic zircons is also present with a Th/U ratio generally less than 0.1. From the CL images of zircons, it is evident that magmatic zircons exhibit weak cathodoluminescence intensity and typical oscillatory zoning, while metamorphic zircons generally show strong cathodoluminescence intensity with no or weak zoning (Figure 3b).

The valid zircon U-Pb ages range mainly from 200 to 600 Ma, with the youngest age being 270 ± 3 Ma and the oldest age being 2565 ± 18 Ma (Figure 4c and Table S2). The concordance of the zircon U-Pb ages is over 93% (Figure 4c). The detrital zircons from the second segment of the Sangonghe Formation are mainly distributed in three intervals, 280–350 Ma (Artinskian–Tournaisian), 380–430 Ma (Givetian–Homerian), and 460–520 Ma (Darrtwilian–Fortunian) (Figure 4d), with the Carboniferous being the main source and followed by the Permian and Devonian. A small number of zircons from the Cambrian, Ordovician, Silurian, and Precambrian are also present.

The QmFLt composition from the Sangonghe Formation sandstones is mainly distributed in the transitional and back-arc provenance areas, as well as the adjacent cutting island arc and transitional island arc margins, indicating a complex provenance with multiple episodes of tectonic activity (Figure 5a). Based on the QmFLt ternary diagram, the provenance of the sandstones is mainly from the retro-arc orogen, indicating that the source area is a volcanic and intermediate intrusive rock-dominated island arc (Figure 5b). According to the QtFL ternary diagram, the samples are mainly distributed in the recycled orogen provenance area, with a large proportion of oceanic source material, suggesting an oceanic subduction background with some mixed provenance characteristics (Figure 5c). From the QpLvLs ternary diagram, the sandstone samples are almost exclusively located in the collisional suture and fold-thrust belt provenance areas, with only a few showing mixed orogenic characteristics (Figure 5d).

5. Discussion

5.1. Provenances of the Dongdaohaizi Depression in Lower Jurassic

Zircon distribution in basin sediments is widespread and has strong stability, which can preserve a large amount of source information. CL images of detrital zircon can clearly reveal information such as internal belts and metamorphic growth, which is beneficial for analyzing the genesis of the parent rock. Combined with zircon U-Pb ages, it can accurately indicate the geological age of the parent rock, and improve the precision of comparison [35–38]. The age combination of zircon in sand bodies supplied by the same provenance must be the same, while there are obvious differences in the age combination of zircon in sand bodies supplied by different provenances. By analyzing the U-Pb ages of detrital zircon in the Badaowan Formation of the study area and determining the genesis of zircon using CL images, the age of the parent rock can be determined, and by comparing with the provenance system, the material source of the sediment can be clarified.

The potential source area of the study area mainly includes the orogenic belts surrounding the basin, such as the eastern Karamaili Mountain, the western Zayir Mountain, and the southern Bogda Mountain. Overall, the zircon ages in the potential source area are mainly concentrated in the range of 200–600 Ma. Among them, the age ranges of the intermediate acidic-acidic eruptive rock, volcanoclastic rock, amphibolite, and other rocks in the Karamaili area include 250–300, 350–380, 400–413, and 475–520, respectively. Additionally, ages 300–350, 388–420, and 485–510 were obtained from rock samples of the Ophiolite belt: basalt, diabase, and gabbro [39–41]. In the Lower Jurassic clastic zircon U-Pb age spectrum of the Dongdaohaizi Depression in this study, three peaks were observed: 280–340 Ma, 400–430 Ma, and 480–520 Ma (Figure 4), which have similar peak intervals with the clastic zircon U-Pb ages in the Karamaili area. It especially contains a peak with high similarity to Karamaili at ~500 Ma, while the Zayir Mountain and the western section of Bogda Mountain do not have this peak age, indicating significant differences. In addition, the Bogda Mountain had not completely uplifted in the Early Jurassic, so the possibility of the Bogda Mountain supplying sources to the study area can be excluded [37,39–44]. Therefore, it is likely that the sediments in the study area represent material brought in by the closure of the Karamaili Ocean.

Additionally, the ternary diagram of the Lower Jurassic sandstones in the Dongdaohaizi Depression shows that the primary source background is composed of transitional reworked orogenic belts, which are consistent with the tectonic background of the Karamaili area (Figure 5). This reflects the processes of island arc collision accompanied by folding and thrusting at the plate margin. Previous studies have found that the Carboniferous was affected by the evolution of the Paleotethys tectonic domain, and the basement was formed by the accretion of volcanic island arcs [45–47]. The most important island arc belt is the Karakorum–Altai–Darbute belt [48,49]. However, the Luliang uplift was a continuous burial background during the Jurassic period and was not a source. The most recent source is the Karakorum-Altai region, so it is the Karakorum-Altai provenance. In addition, the rock debris is mainly composed of volcanic rock debris, and there is a large number of tuffaceous debris, while the proportion of sedimentary and metamorphic rock debris is relatively small, indicating that the main source of the basin-margin Karakorum orogeny is volcanic rocks. Previous studies of sedimentary features and ancient rivers in the northwest indicate that they have shallow-water traction flow characteristics and the ability to transport over long distances [22]. Therefore, we believe that the Lower Jurassic in the Dongdaohaizi Depression received a large amount of Karamaili provenance sediment from the eastern margin of the Junggar basin, which can be used to study the evolutionary process of the Karamaili Ocean.

Based on the ages of sandstone detrital zircons from the Badaowan Formation to the Sangonghe Formation, the three main peaks of zircon age spectra are consistent between them and exhibit a characteristic age range of 490–520 Ma, which is similar to the mother rocks from Karamaili region. Therefore, the study area in the Lower Jurassic is mainly supplied with sediment from a stable source region in the Karamaili Orogenic Belt. It is worth noting that among the zircon ages of the Badaowan Formation, 36 zircons are from the Permian period, accounting for 36% of the total, while 24 zircons are from the Carboniferous period, accounting for 24% of the total (Table S2). The zircon results of the Sangonghe Formation show that 18 zircons are from the Permian period, accounting for 18% of the total, while 50 zircons are from the Carboniferous period, accounting for 50% of the total (Table S2). From the early to late Jurassic, the Permian zircons decreased, while the Carboniferous zircons increased significantly, indicating a trend of younger to older ages in the stratigraphic sequence and suggesting that older rocks from the deeper source region have continued to erode and expose over time. In addition, the sedimentary sequence fines upwards during the lower Jurassic, which may indicate an increasing distance of sources from sediment to the basin caused by basin extension.

Based on the Dickinson provenance analysis, it is suggested that the source area of the Kelamayi Mountains during the Lower Jurassic was subjected to a background of collisional sutures and folding-thrusting, indicating a continuous compression and uplift environment. In previous traditional geological studies in the eastern Junggar Basin, based on methods such as the tectonic stratigraphic layering [50], the changing of sedimentary cycles and migration of sedimentary centers [51,52], and the planar changes of sedimentary facies [53], it was determined that the Early Jurassic was a stage of intra-cratonic sagging. By analyzing the original basin properties through the geometric characteristics of the tectonic structure profile, it was considered that the basin was a sag-type basin caused by peripheral squeezing [48,54–56]. From the burial history of the basin, geochemical analysis, and field geological profile observations, it was suggested that the basin was an intracratonic sag basin [57,58]. Although there are still discrepancies in the evidence obtained in some areas, overall, the Early Jurassic Junggar Basin was a stage of compression and sagging under the control of the Yanshanian movement caused by the closure of the Okhotsk Ocean during the Jurassic–Cretaceous.

In the Zhantenggou area of the eastern Junggar Basin, the unconformable contact between the Jurassic Badaowan Formation and the Triassic Xiaoquangou Group ($J_1b/T_{2\text{-}3}xq$) was discovered, indicating a significant tectonic uplift event during the Late Triassic to Early Jurassic with clear regional tectonic background and geological responses such as folding and faulting, representing the continuous tectonic uplift and erosion of the eastern Junggar orogenic belt [59]. The tectonic uplift event during the Late Triassic to Early Jurassic (210 to 180 Ma) was identified through in-situ apatite fission track analysis [60]. Similarly, the tectonic uplift event during the Middle Triassic to Early Jurassic (240 to 180 Ma) was recognized through seismic profiles combined with apatite fission track data analysis [61]. The evidence above indicates the continuous tectonic uplift and erosion of the eastern Junggar orogenic belt. The continuous tectonic uplift resulted in the continuous exposure of deeper strata in the source area, and older rock debris was transported to the study area.

During the late Triassic to early Jurassic, the grid-like tectonic pattern of the sedimentary layers was filled in and the basin began to contract under the influence of the Indonesian movement, leading to a shrinking lacustrine basin and distribution of swamps [48,62]. In the late Early Jurassic, the basin base subsided again, the lacus expanded, and coal seams developed in the shallow lacus and swamp sedimentary environment of the basin. In the early Middle to Late Jurassic, the mountain-building activity began to resume, and the peripheral thrust belts oscillated back and forth and thrust into the basin, causing the basin to shrink inward and resulting in large-scale peat swamp sedimentation throughout the basin. Based on field outcrop and core observations, various facies markers were identified, and it was found that braid-deltaic plains and frontiers with a large number of branching river channels developed from the Karamaili area of East Junggar to the study area [63–65]. Under this environment, the river channels continuously eroded and destroyed the mountains, causing the drainage area to increase and older layers to be exposed and transported into the study area.

5.2. Tectonic Implications

The analysis results show that all the sample points in the QFL diagram fall into the area of the retro-orogenic belt (Figure 5), and the samples are biased toward the continental source area. Meanwhile, the low content of plagioclase and the high content of quartz (including chert) in the clastic rocks indicate that their source area mainly comes from the retro-orogenic belt. In the QmFLt diagram, the samples are mainly distributed in the source areas of quartz retro-orogenic and transitional retro-orogenic (6-b), which are mostly close to the magma island arc source area, indicating that the source area contains a large number of volcanic rocks and intermediate-acid intrusive rocks. Both the QFL and QmFLt diagrams indicate that the source area is basically a retro-orogenic belt, indicating that the source area belongs to a collisional suture zone or a fold-thrust belt. Based on the regional geological background and the location of the sample points, the source area in the study area is an evolution process of the cut island arc and transitional arc towards the transitional retro-orogenic belt and the detrital retro-orogenic belt (collisional orogenic belt). Combining the characteristics of the peak age of zircon, it reflects the process of multiple oceanic basin extensions, subductions, collisions, and compressional over thrusting in the Eastern Junggar region.

In this study, zircon grains from 460–540 Ma were used to indicate the timing of subduction and accretion of the Karamaili Ocean in the late Cambrian to early Ordovician, with peak magmatism occurring around 520 Ma. In the late Cambrian, the northern branch of the East Junggar Ocean, the paleo-Karamaili Ocean, subducted and was consumed during the Devonian, forming the preliminary Karamaili orogenic belt. Some previous studies also support this conclusion. The age range of 490–520 Ma is unique to the Karamaili region and is likely derived from the reworked part of the Paleozoic strata [53]. Ophiolites in the East Junggar Altay area formed in the Cambrian-early Ordovician and include diorite (489 $\pm$ 4 Ma [66])) and gabbro (503 $\pm$ 7 Ma and 496 $\pm$ 6 Ma [67]). Jian [66] obtained two SHRIMP U-Pb zircon ages of diorite from the Zhaheba ophiolite in the East Junggar region, which was 489 $\pm$ 4 Ma, and they considered this to be the formation age of the ophiolite. Fang [68] obtained a peak age of 514 $\pm$ 5 Ma for the diorite from the Karamaili ophiolite in the East Junggar region using LA-ICP-MS zircon U-Pb dating. Combining the ages of the Zhaheba and Altay ophiolites obtained in previous studies (489 $\pm$ 4 Ma and 503 $\pm$ 7 Ma [66,67]), the formation age of the Beitaishan ophiolite was determined to be 494 $\pm$ 3 Ma. QFL diagram analysis results indicate that the samples all fall within the orogenic belt of reworked strata (Figure 5), with samples tending towards an oceanic source, while feldspar content is low and quartz (including chert) content is high, indicating that the Karamaili region is mainly derived from the reworked orogenic belt. It is a mantle material from oceanic subduction to continental arc with volcanic island arc characteristics, forming recycled oceanic debris.

The latest zircon dating results from this study constrain the extension and convergence processes of the limited ocean basin of Karamaili Ocean from the Late Silurian to Early Carboniferous periods to be within 360–440 Ma. Jian [66] obtained two groups of SHRIMP U-Pb ages of 406 $\pm$ 4 Ma from the zircons of gabbros in the Zhahaba ophiolite complex in eastern Junggar and suggested that the occurrence of this age group represented a magmatic thermal event. Zhang [69] obtained a zircon age of 409 $\pm$ 9 Ma from the gabbros in Zhahaba, and based on previous research results, they concluded that the Zhahaba-Almantai region in eastern Junggar contained Middle Ordovician to Early Devonian ophiolites, reflecting the background of continuous oceanic subduction. Fang [68] studied the formation age of the Karamaili ophiolite in eastern Junggar and obtained a peak zircon age of 406 ± 2 Ma by LA-ICP-MS U-Pb dating of gabbros, which they believed represented the age of the Karamaili ophiolite formation. Liu [70] also found a younger group of zircons (412 ± 13 Ma) in the gabbros, which have ages similar to the granite porphyry intrusions (407 ± 2 Ma) in the nearby basalts. They speculated that these ages may be related to magmatic thermal events in the island arc area under compression during the convergence and closure of the Zhahaba-Almantai-North Tashan ocean basin. The geochemical characteristics of the granite porphyries discovered in the North Tashan ophiolitic mélange suggest that they may have formed in an island arc area with thickened crust during the subduction closure of the ocean basin, and therefore, the formation age of the granite porphyries at 407 ± 2 Ma marks the convergence and closure of the Almantai ocean basin, entering the collisional tectonic evolution stage from the Late Silurian to Early Devonian periods. The triangular diagrams reflecting the re-collision orogen indicate that the source area belongs to a collisional suture zone. The obtained age peak at ~400 Ma is similar to the results of these studies, reflecting the tectonic events of convergence and closure from the Late Silurian to Early Devonian periods, followed by the collisional tectonic evolution stage. During this time, volcanic and magmatic activities were relatively active, and the volcanic rocks of the island arc were weathered and eroded to form clastic rocks through nearby transport and accumulation.

The zircon age range of 240–340 Ma indicates the complete disappearance of the Eastern Junggar Ocean during the late Carboniferous to the Triassic period [71]. The LA-ICP-MS zircon U-Pb age of the Laoyemiao rhyolite shows that the crystallization age of the rhyolite is (311.6 ± 3.1) Ma, indicating its formation in the late Carboniferous. The rhyolite has A-type granite characteristics, with high Ga/Al, Zr, Nb, Ga, Y, and Ce, low Sr, and a significant negative Eu anomaly. It is classified as an A2-type granite and formed in a post-collisional environment, marking the complete closure of the basin in the eastern Junggar area [72]. Detailed petrological, geochemical, zircon U-Pb chronology and Sr-Nd-Pb isotope composition studies were conducted on the late Carboniferous bimodal volcanic in the Karamaili orogenic belt in eastern Junggar. The volcanic rocks were considered to have formed in the early late Carboniferous at 320.2 ± 4.2 Ma. The bimodal volcanic rocks were produced in a post-collisional tectonic environment, where the sinking of the oceanic crust caused an upwelling of the asthenosphere, resulting in partial melting of the overlying mantle, and the intrusion of the lower crust caused partial melting, leading to the eruption of the bimodal volcanic rocks. The occurrence of the bimodal volcanic rocks marks the end of the orogenic process in the Karamaili area of eastern Junggar [73]. The age and petrogeochemistry of the alkaline granite in the Ashudas area of the northeast margin of eastern Junggar were investigated by SHRIMP zircon U-Pb dating, indicating a crystallization age of (319.3 ± 2.5) Ma, with typical A-type granite characteristics. Its formation marked the end of the orogenic phase in the northern margin of eastern Junggar and the beginning of an intra-plate extensional environment. The Tawibask granite porphyry has high SiO2, quasi-aluminous-weakly peraluminous, and calc-alkaline I-type granite characteristics, with weighted average ages of 301.3 ± 2.5 Ma (MSWD = 0.33) and 310.7 ± 3.6 Ma (MSWD = 0.75), indicating that the late Carboniferous (310~301 Ma) in the eastern Junggar region was in a post-collisional tectonic setting with mixed crust-mantle and incremental growth characteristics [74]. The Dickinson triangle reflects a retro-arc orogenic belt, indicating typical collisional suture and fold-thrust belt source characteristics, indicating that the Karamaili area of eastern Junggar has entered a comprehensive and sustained compressive uplift background. This study demonstrates a peak in the Late Carboniferous to Early Permian, indicating the end of the eastern Junggar orogeny. During the Jurassic period, the pre-existing multiple sets of volcanic rock weathering debris and peripheral volcanic debris rocks were uplifted to the surface, weathered, and eroded again, becoming the source rocks of Jurassic detrital rocks [49,75,76]. In the Jurassic, the closure of the Paleo-Tethys Ocean and the opening of the Neo-Tethys Ocean affected western China and central Asia, which were in the stage of basin extension and faulting. Under this background, the Karamaili area continued to uplift in the Early Jurassic, developing mountain basins, and providing a large amount of detrital material for the area [77,78].

In summary, the detrital zircon age spectrum of the Early Jurassic in the Dongdaohaizi Depression fully reflects the tectonic characteristics of the provenance area in the Karamaili Mountains region. The ages record the East Junggar Ocean's extension-collapse cycles during the Cambrian to Early Silurian; the limited Karamaili Ocean's subduction and convergence during the Late Silurian to Early Carboniferous; and the complete disappearance of the Paleo-Asian Ocean during the Late Carboniferous to Triassic. Then the North Tianshan Ocean basin underwent a transformation from an oceanic basin to a foreland basin during the convergent and compressive stages of the extension-collapse cycles. This comprehensive record witnessed the complete evolution process of the Paleo-Asian Ocean and provides valuable insights into the tectonic evolution of the study area.

6. Conclusions

(1) The sedimentary characteristics of the Lower Jurassic in the Dongdaohaizi Depression of the Junggar Basin indicate a transitional and episodic provenance from a collisional orogen with an oceanic-continental subduction background.

(2) The age ranges of the Badaowan Formation are 240–340 Ma, 360–440 Ma, and 480–540 Ma, while those of the Sangonghe Formation are 260–340 Ma, 370–440 Ma, and 460–520 Ma. The youngest detrital zircon age is 241 $\pm$ 2 Ma, indicating the earliest limit of sedimentation in the Early Permian.

(3) During the Early Jurassic, the consistent subduction of the residual East Junggar Ocean induced continuous uplift in the Karamaili region, resulting in an increasing exposure of deep-seated rocks to provide sedimentary material.

(4) The Karamaili Ocean, as part of the Paleo-Asian Ocean, experienced three evolutionary stages: Cambrian-Early Silurian (460–540 Ma), Late Silurian-Early Carboniferous (360–440 Ma), and Late Carboniferous-Triassic (240–340 Ma).

Supplementary Materials: The following supporting information can be downloaded at: https://www.mdpi.com/article/10.3390/jmse11071375/s1, Table S1: Components and contents of Badaowan and Sangonghe Formation samples in the Dongdaohaizi Depression; Table S2: LA-ICP-MS zircon U-Pb dating results of sandstones from the Badaowan and Sangonghe formations in Dongdaohaizi Depression, Junggar basin.

Author Contributions: Conceptualization, Y.G. and F.L.; methodology, G.Z. and R.G.; writing—original draft preparation, Y.G. and F.L.; writing—review and editing, Y.G., S.L. (Songtao Li) and S.L. (Shengqian Liu); investigation, Z.Z., S.C. and Z.X.; visualization, L.L. and H.Z. All authors have read and agreed to the published version of the manuscript.

Funding: This research was funded by Sinopec Science and Technology Projects (P21077-2; YKK2212; YJQ2301).

Institutional Review Board Statement: Not applicable.

Informed Consent Statement: Not applicable.

Acknowledgments: We acknowledge the Sinopec Science and Technology Projects (P21077-2; YKK2212; YJQ2301) for funding this study. We thank Xiaoliang We for the fantastic devices. Thanks to the 4 anonymous reviewers for their valuable suggestions.

Conflicts of Interest: The authors declare no conflict of interest.

References

1. Jahn, B.-M.; Wu, F.; Chen, B. Massive granitoid generation in Central Asia: Nd isotope evidence and implication for continental growth in the Phanerozoic. *Epis. J. Int. Geosci.* **2000**, *23*, 82–92. [CrossRef] [PubMed]
2. Kroener, A.; Rojas-Agramonte, Y. The Altaids as Seen by Eduard Suess, and Present Thinking on the Late Mesoproterozoic to Palaeozoic Evolution of Central Asia. *Austrian J. Earth Sci.* **2014**, *107*, 156–168.

3. Kovalenko, V.I.; Yarmolyuk, V.V.; Kovach, V.P.; Kotov, A.B.; Kozakov, I.K.; Salnikova, E.B.; Larin, A.M. Isotope provinces, mechanisms of generation and sources of the continental crust in the Central Asian mobile belt: Geological and isotopic evidence. *J. Asian Earth Sci.* **2004**, *23*, 605–627. [CrossRef]
4. Safonova, I.Y. Geochemical evolution of intraplate magmatism in the Paleo-Asian Ocean from the Late Neoproterozoic to the Early Cambrian. *Petrology* **2008**, *16*, 492. [CrossRef]
5. Xiao, W.; Santosh, M. The western Central Asian Orogenic Belt: A window to accretionary orogenesis and continental growth. *Gondwana Res.* **2014**, *25*, 1429–1444. [CrossRef]
6. Xiao, W.; Han, C.; Yuan, C.; Sun, M.; Lin, S.; Chen, H.; Li, Z.; Li, J.; Sun, S. Middle Cambrian to Permian subduction-related accretionary orogenesis of Northern Xinjiang, NW China: Implications for the tectonic evolution of central Asia. *J. Asian Earth Sci.* **2008**, *32*, 102–117. [CrossRef]
7. Xiao, W.; Windley, B.F.; Badarch, G.; Sun, S.; Li, J.; Qin, K.; Wang, Z. Palaeozoic accretionary and convergent tectonics of the southern Altaids: Implications for the growth of Central Asia. *J. Geol. Soc.* **2004**, *161*, 339–342. [CrossRef]
8. Sengör, A.M.C.; Natal'In, B.A. Turkic-type orogeny and its role in the making of the continental crust. *Annu. Rev. Earth Planet. Sci.* **1996**, *24*, 263–337. [CrossRef]
9. Şengör, A.M.C.; Natal'in, B.A. Phanerozoic analogues of Archaean oceanic basement fragments: Altaid ophiolites and ophirags. *Dev. Precambrian Geol.* **2004**, *13*, 675–726.
10. Yakubchuk, A.; Seltmann, R.; Shatov, V.; Cole, A. The Altaids: Tectonic evolution and metallogeny. *SEG Discov.* **2001**, *1*, 1–14. [CrossRef]
11. Allen, M.B.; Windley, B.F.; Zhang, C. Palaeozoic collisional tectonics and magmatism of the Chinese Tien Shan, central Asia. *Tectonophysics* **1993**, *220*, 89–115. [CrossRef]
12. Windley, B.F.; Allen, M.B.; Zhang, C.; Zhao, Z.Y.; Wang, G.R. Paleozoic accretion and Cenozoic redeformation of the Chinese Tien Shan Range, central Asia. *Geology* **1990**, *18*, 128–131. [CrossRef]
13. Şengör, A.M.C.; Natal'in, B.A.; Burtman, V.S. Evolution of the Altaid tectonic collage and Palaeozoic crustal growth in Eurasia. *Nature* **1993**, *364*, 299–307. [CrossRef]
14. Coleman, R.G. Continental growth of northwest China. *Tectonics* **1989**, *8*, 621–635. [CrossRef]
15. Liu, X.; Xiao, W.; Xu, J.; Castillo, P.R.; Shi, Y. Geochemical signature and rock associations of ocean ridge-subduction: Evidence from the Karamaili Paleo-Asian ophiolite in east Junggar, NW China. *Gondwana Res.* **2017**, *48*, 34–49. [CrossRef]
16. Li, D.; He, D.; Sun, M.; Zhang, L. The Role of Arc-Arc Collision in Accretionary Orogenesis: Insights From ∼320 Ma Tectono-sedimentary Transition in the Karamaili Area, NW China. *Tectonics* **2020**, *39*, e2019TC005623. [CrossRef]
17. Zhang, B.; Chen, C.; Gong, X.; Yalikun, Y.; Kaheman, K. The Kamusite A2-type granites in the Karamaili tectonic belt, Xinjiang (NW China): Tracing staged postcollisional delamination in the eastern Junggar. *Geol. Mag.* **2020**, *158*, 723–748. [CrossRef]
18. Gilder, S.; Zhao, X.; Coe, R.; Meng, Z.; Courtillot, V.; Besse, J. Paleomagnetism and tectonics of the southern Tarim basin, northwestern China. *J. Geophys. Res. Solid Earth* **1996**, *101*, 22015–22031. [CrossRef]
19. Gao, Y.; Zhang, S.; Zhao, H.; Ren, Q.; Yang, T.; Wu, H.; Li, H. North China block underwent simultaneous true polar wander and tectonic convergence in late Jurassic: New paleomagnetic constraints. *Earth Planet. Sci. Lett.* **2021**, *567*, 117012. [CrossRef]
20. Sharps, R.W. *Paleomagnetism and Tectonics of Northwest China*; Stanford University: Stanford, CA, USA, 1990.
21. Zhang, L.; Dengfa, H.; Zejun, Y.; Di, L.I. Tectonic relationship between the Kelameili range and the Dajing depression: Insights into the Carboniferous tectonic-sedimentary framework. *Pet. Explor. Dev.* **2020**, *47*, 30–45. [CrossRef]
22. Zheng, S. Sedimentary Pattern of the Shallow-Water Delta in the Sangonghe Formation of Central Junggar Basin and Its Significance for Hydrocarbon Exploration. *Spec. Oil Gas Reserv.* **2019**, *26*, 87–93.
23. Chew, D.M.; Spikings, R.A. Geochronology and Thermochronology Using Apatite: Time and Temperature, Lower Crust to Surface. *Elements* **2015**, *11*, 189–194. [CrossRef]
24. Feng, Y.; Coleman, R.G.; Tilton, G.; Xiao, X. Tectonic evolution of the west Junggar region, Xinjiang, China. *Tectonics* **1989**, *8*, 729–752. [CrossRef]
25. Buckman, S.; Aitchison, J.C. Tectonic evolution of Palaeozoic terranes in west Junggar, Xinjiang, NW China. *Geol. Soc. Lond. Spec. Publ.* **2004**, *226*, 101–129. [CrossRef]
26. Gao, R.; Xiao, L.; Pirajno, F.; Wang, G.-c.; He, X.-x.; Yang, G.; Yan, S.-w. Carboniferous–Permian extensive magmatism in the West Junggar, Xinjiang, northwestern China: Its geochemistry, geochronology, and petrogenesis. *Lithos* **2014**, *204*, 125–143. [CrossRef]
27. Chen, Y.; Xiaogan, C.; Han, Z.; Li, C.; Ma, Y.; Wang, G. Fault characteristics and control on hydrocarbon accumulation of middle-shallow layers in the slope zone of Mahu sag, Junggar Basin, NW China. *Pet. Explor. Dev.* **2018**, *45*, 1050–1060. [CrossRef]
28. Andersen, T. Correction of common lead in U-Pb analyses that do not report 204Pb. *Chem. Geol.* **2002**, *192*, 59–79. [CrossRef]
29. Sircombe, K.N. Tracing provenance through the isotope ages of lit-toral and sedimentary detrital zircon, eastern Australia. *Sediment. Geol.* **1999**, *124*, 47–67. [CrossRef]
30. Sudar, V.; Aljinović, D.; Smirčić, D.; Barudžija, U. Composition and provenance of Gröden sandstone from the Velebit Mts. *Rudarsko-Geološko-Naftni Zbornik* **2016**, *31*, 53–67. [CrossRef]
31. Ludwig, K. RISOPLOT 2.49: A Geochronological Toolkit for Microsoft Excel. *Berkeley Geochronol. Cent. Spec. Publ.* **2001**, *1a*, 1–58.
32. Li, Z.; Li, R.; Sun, S.; Jiang, M.; Zhang, W. Detrital composition and provenance tectonic attributes of Jurassic sandstones, south Hefei basin. *Acta Petrol. Sin.* **1999**, *15*, 438–445.

33. Ingersoll, R.V.; Bullard, T.F.; Ford, R.L. The effect of grain size on detrital modes: A testof the Gazzi-Dickinson point-counting method. *J. Sediment. Petrol.* **1984**, *54*, 103–116.
34. Dickinson, W.R. Interpreting detrital models of graywacke and arkose. *J. Sediment Petrol.* **1970**, *40*, 695–707.
35. Guangwen, H.; Jiayong, P.; Guangnan, H.; Fei, X.; Dehai, W.; Fujun, Z. Zircon Chronological Characteristics and Geological Significance of Sedimentary Rocks of Badaowan Formation in Mengqiguer Area, Xinjiang. *Xinjiang Geol.* **2021**, *39*, 210–219.
36. Ni, M. Source Analysis and Tectonic Significance of Middle-lowermesozoic in Northwest Margin of Junggar Basin: Evidence Fromdetrital Zircon U-pb Age. Master's Thesis, China University of Petroleum (Beijing), Beijing, China, 2019.
37. Wang, X.; Cai, K.; Sun, M.; Xiao, W.; Xia, X.; Wan, B.; Bao, Z.; Wang, Y. Two contrasting late Paleozoicmagmatic episodes in the northwestern Chinese Tianshan Belt, NWChina: Implication for tectonic transition from plate convergence tointra-plate adjustment during accretionary orogenesis. *J. Ofasian Earth Sci.* **2017**, *153*, 118–138. [CrossRef]
38. Hartanto, P.; Alam, B.Y.C.S.; Lubis, R.F.; Hendarmawan, H. The Origin and Quality of the Groundwater of the Rawadanau Basin in Serang Banten. *Indonesia. Rud. Geološko Naft. Zb.* **2021**, *36*, 11–24. [CrossRef]
39. Liu, X. The Evolution of Dynamic Structural Belt in Kalamaili Mountains in the Junggar Basin., 2016. Ph.D. Thesis, Southwest Petroleum University, Chengdu, China, 2016.
40. Zhang, Y.; Pe-Piper, G.; Piper, D.J.W.; Guo, Z. Early Carboniferous collision of the Kalamaili orogenic belt, North Xinjiang, and its implications: Evidence from molasse deposits. *Bulletin* **2013**, *125*, 932–944. [CrossRef]
41. Zhang, Y.; Guo, Z.; Pe-Piper, G.; Piper, D.J.W. Geochemistry and petrogenesis of Early Carboniferous volcanic rocks in East Junggar, North Xinjiang: Implications for post-collisional magmatism and geodynamic process. *Gondwana Res.* **2015**, *28*, 1466–1481. [CrossRef]
42. Ji, H.; Tao, H.; Wang, Q. Early to middle Jurassic tectonicevolution of the Bogda Mountains, Northwest China: Evidence fromsedimentology and detrital zircon geochronology. *J. Asian Earth Sci.* **2018**, *153*, 57–74. [CrossRef]
43. Han, B.F.; Guo, Z.J.; Zhang, Z.C. Age, geochemistry, andtectonic implications of a late Paleozoic stitching pluton in the northTian Shan suture zone, western China. *Geol. Soc. Ofamerica Bull.* **2010**, *122*, 627–640. [CrossRef]
44. Wali, G.; Wang, B.; Cluzel, D. Carboniferous-Early Permianmagmatic evolution of the Bogda Range (Xinjiang, NW China): Implications for the Late Paleozoic accretionary tectonics of the SWCentral Asian orogenic belt. *J. Asian Earth Sci.* **2018**, *153*, 238–251. [CrossRef]
45. Filippova, I.B.; Bush, V.A.; Didenko, A.N. Middle Paleozoic subduction belts: Theleading factor in the formation of the Central Asian fold-and-thrust belt. *Russ. J. Earth Sci.* **2001**, *3*, 405–426. [CrossRef]
46. Mossakovsky, A.A.; Ruzhentsev, S.V.; Samygin, S.G.; Kheraskova, T.N. The CentralAsian fold belt: Geodynamic evolution and formation history. *Geotectonics* **1993**, *26*, 455–473.
47. Xiao, W.J.; Windley, B.F.; Allen, M.F.; Han, C.M. Paleozoic multiple accretionary andcollisional tectonics of the Chinese Tianshan orogenic collage. *Gondwana Res.* **2013**, *23*, 1316–1341. [CrossRef]
48. He, D.; Zhang, L.; Wu, S.; Li, D.; Zhen, Y. Tectonic evolution stages and features of the Junggar Basin. *Oil Gas Geol.* **2018**, *39*, 845–861.
49. Li, D.; He, D.; Fan, C.; Xiang, K.; Jin, L. Early Permian Post-collisional Magmatic Events, East Junggar: Constraints From Zircon Shrimp U-pb Age, Geochemistry And Hf Isotope Of Rhyolite In The Yundukala Area. *Acta Petrol. Sin.* **2013**, *1*, 317–337.
50. Chen, X.; Lu, H.; Shu, L.; Wang, H.; Zhang, G. Study on Tectonic Evolution of Junggar Basin. *Geol. J. China Univ.* **2002**, *3*, 257–267.
51. Chen, F.; Zhang, G.; Chen, Z. Unconformity Analysis and Its Significance in The Study of Continental Basin Tectonics. *Geoscience* **2004**, *3*, 269–275.
52. Qu, G.-s.; MA, Z.-j.; Chen, X.-f.; Li, T.; Zhang, N. On structures and evolutions in Junggar Basin. *Xinjiang Pet. Geol.* **2009**, *30*, 1–5.
53. Zhang, C.; He, D.; Wu, X.; Shi, X. Formation and evolution of multicycle superimposed basins in Junggar Basin. *China Pet. Explor.* **2006**, *11*, 47.
54. He, D.; Zhou, L.; Tang, Y.; Wu, X.; Du, S. Characteristics of unconformity between the Xishanyao Formation and Toutunhe Formation of Middle Jurassic in Junggar Basin and its significance in petroleum exploration. *J. Palaeogeogr.* **2007**, *4*, 387–396.
55. Wu, K.; Paton, D.; Zha, M. Unconformity structures controlling stratigraphic reservoirs in the north-west margin of Junggar basin, North-west China. *Front. Earth Sci.* **2013**, *7*, 55–64. [CrossRef]
56. Han, X.; Ayiguli, W.U. Tectonic Framework and Stucutral Patterns in Peripheral Eastern Junggar Basin. *Xinjiang Pet. Geol.* **2001**, *22*, 202.
57. Wang, S.; Zou, C.; Hou, L.; Wei, Y.; Luo, X.; Guo, Z. Petroleum geological characteristics of gas accumulation in carboniferous volcanics and prospect for gas exploration, Eastern Junggar Basin. *Earth Sci. Front.* **2013**, *2*, 226–236.
58. Cai, Z.; Chen, F.; Jia, Z. Types and Tectonic Evolution of Junger Basin. *Earth Sci. Front.* **2003**, *7*, 431–440.
59. Nie, L.; Ma, J.; Tang, X. Meso-Cenozoic tectonic events and their petroleum geological significance in Zhangpenggou area, eastern Junggar Basin. *Lithol. Reserv.* **2023**, *35*, 81–91.
60. Song, J.; Qin, M.; Cai, Y.; Guo, Q.; He, Z.; Liu, Z.; Cao, X.; Chen, Z. Uplift-Denudation of Orogenic Belts Control on the Formation of Sandstone Type Uranium(U) Deposits in Eastern Junggar, Northwest China: Implications from Apatite Fission Track (AFT). *Earth Sci.* **2019**, *44*, 3910–3925.
61. Wu, Z.; Han, X.; JI, H. Mesozoic-Ceno-zoic tectonic events of eastem Junggar Basin, NW China andtheir significance for uranium mineralization; Insights fromseismic profiling and AFT dating analysis. *Ore Geol. Rev.* **2021**, *139*, 104488. [CrossRef]

62. Xinzhi, Z.; Linhao, F.; Tao, W.; Yunfa, M.; Mingzhen, Z.; Xuelian, W.; Peizong, L.; Xiujuan, H.; Ruoyuan, Q.; Han, Y. Palynological assemblages and palaeoclimate across the Triassic-Jurassic boundary in the Haojiagou section, southern Junggar Basin. *Chin. J. Geol.* **2022**, *57*, 1161–1176.
63. Song, C.; Cheng, C.; Qiao, Y. Sedimentary Characteristics of Jurassic Toutunhe Formation in Block 4 Central Junggar Basin. *Adv. Geosci.* **2019**, *9*, 1229–1236. [CrossRef]
64. Xia, T. Reservoir Characteristics of the Badaowan Formation in Central Junggar Basin. Master's Thesis, China University of Petroleum (Qingdao), Qingdao, China, 2018.
65. Zhu, X.; Li, S.; Wu, D.; Zhu, S.; Dong, Y.; Zhao, D.; Wang, X.; Zhang, Q. Sedimentary characteristics of shallow-water braided delta of the Jurassic, Junggar basin, Western China. *J. Pet. Sci. Eng.* **2017**, *149*, 591–602. [CrossRef]
66. Jian, P.; Liu, D.-y.; Zhang, Q.; Zhang, F.-q.; Shi, Y.-r.; Shi, G.-h.; Zhang, L.-q.; Tao, H. Shrimp Dating of Ophiolite And Leucocratic Rocks Within Ophiolite. *Earth Sci. Front.* **2003**, *4*, 439–456.
67. Xiao, W.; Windley, B.F.; Yan, Q.; Qin, K.; Chen, H.; Yuan, C.; Sun, M.; Li, J.; Sun, S. SHRIMP zircon age of the Aermantai ophiolite in the North Xinjiang area, China and its tectonic implications. *Acta Geol. Sin.* **2006**, *80*, 32–37.
68. Fang, A.; Wang, S.; Zhang, J.; Zang, M.; Fang, J.; Hu, J. The U-Pb ages of zircons from the gabbro in the Kalamaili ophiolite, North Xinjiang and its tectonic significances. *Chin. J. Geol.* **2015**, *50*, 140–154.
69. Zhang, Y. The Study About the Composition, the Structure, Theemplacement Mechanism and Significance of Tectonic of the Armantai Ophiolite Melange, East Junggar, Xinjiang, China. Ph.D. Thesis, Chang'an University, Xi'an, China, 2013.
70. Liu, Y. Early Paleozoic ophiolite SHRIMP U-Pb dating and its Genetic Types & Tectonic Setting in eastern Junggar, Xinjiang. Ph.D. Thesis, China University of Geosciences, Beijing, China, 2016.
71. Xiong, S.; Zhang, Z.; Li, G.; Liu, R.; Hua, X.; Zhao, F.; Zhou, P.; Li, G. Zircon U-Pb Dating, Geochemical Characteristics of Alkali-granites in Laoyemiao Area, Eastern Junggar, and Geological Significance. *Geol. Rev.* **2019**, *65*, 221–231.
72. Luo, T.; Chen, S.; Liao, Q.A.; Chen, J.; Hu, C.; Wang, F.; Tian, J.; Wu, W. Geochronology, Geochemistry and Geological Significance of the Late Carboniferous Bimodal Volcanic Rocks in the Eastern Junggar. *Earth Sci.* **2016**, *41*, 1845–1862.
73. Alimujiang, A.; Gong, X.; Li, X.; Zheng, F.; Shang, M.; Muzhapaer, M. LA-ICP-MS Zircon U-Pb Dating, Geochemical Characteristics and Tectonic Significance of Ashudas Late Carboniferous Alkaline Granite in Northeast Margin of Eastern Junggar, Xinjiang. *Xinjiang Geol.* **2020**, *38*, 184–191.
74. Wei, T.; Rukui, L.; Ling, G.; Yang, L.; Gang, H.; Feng, Y. Zircon U-Pb dating, geochemistry and tectonic significance of the volcanic rocks in Liushugou Formation, East Junggar. *Chin. J. Geol.* **2022**, *57*, 782–808.
75. Jin, J.; Wang, J.; Liu, J.; Tuxun'ayi, T.; Ji, H.; Jia, H.; Fang, C.; Li, C. Characteristic and distribution of lithology-lithofacies of deep Carboniferous reservoirs in the Ke-Bai fractured zone of the northwestern margin in Junggar Basin. *J. Northwest Univ.* **2018**, *48*, 238–245.
76. Liu, J.; Yang, Y. Comparison of Sedimentary Characteristics on Both Sides of Karamaili Ophiolite Belt in Eastern Junggar, Xinjiang. *Adv. Geosci.* **2020**, *10*, 758–770. [CrossRef]
77. Zheng, M.; Tian, A.; Yang, T.; He, W.; Chen, L.; Wu, H.; Ding, J. Structural evolution and hydrocarbon accumulation in the eastern Junggar Basin. *Oil Gas Geol.* **2018**, *39*, 907–917.
78. Li, D.; He, D.; Tang, Y.; Fan, C.; Kong, Y. Genesis of Early Carboniferous volcanic rocks of the Di'nan uplift in Junggar Basin: Constraints to the closure time of Kalamaili ocean. *Acta Petrol. Sin.* **2015**, *28*, 2340–2354.